Biophysical Journal
Article

Biophysical Society

Millimeter Wave Radiation Activates Leech Nociceptors via TRPV1-Like Receptor Sensitization

Sergii Romanenko,[1,*] Alan R. Harvey,[2,4] Livia Hool,[2,3] Shuting Fan,[1,5] and Vincent P. Wallace[1]
[1]Department of Physics and [2]School of Human Sciences, The University of Western Australia, Perth, Western Australia, Australia; [3]Victor Chang Cardiac Research Institute, Sydney, New South Wales, Australia; [4]Perron Institute for Neurological and Translational Science, Perth, Western Australia, Australia; and [5]College of Electronic Science and Technology, Shenzhen University, Shenzhen, China

ABSTRACT There is evidence that millimeter waves (MMWs) can have an impact on cellular function, including neurons. Earlier in vitro studies have shown that exposure levels well below the recommended safe limit of 1 mW/cm^2 cause changes in the action potential (AP) firing rate, resting potential, and AP pulse shape of sensory neurons in leech preparations as well as alter neuronal properties in rat cortical brain slices; these effects differ from changes induced by direct heating. In this article, we compare the responses of thermosensitive primary nociceptors of the medicinal leech under thermal heating and MMW irradiation (80–170 mW/cm^2 at 60 GHz). The results show that MMW exposure causes an almost twofold decrease in the threshold for activation of the AP compared with thermal heating (3.9 $\pm$ 0.4 vs. 8.3 $\pm$ 0.4 mV, respectively). Our analysis suggests that MMWs-mediated threshold alterations are not caused by the enhancement of voltage-gated sodium and potassium conductance. We propose that the reduction in AP threshold can be attributed to the sensitization of the transient receptor potential vanilloid 1-like receptor in the leech nociceptor. In silico modeling supported our experimental findings. Our results provide evidence that MMW exposure stimulates specific receptor responses that differ from direct thermal heating, fostering the need for additional studies.

INTRODUCTION

Applications of artificially generated millimeter wave (MMW) radiation (30–300 GHz) are growing rapidly. Point-to-point wireless communications links, local area networks, security screening systems, and even nonlethal crowd control weapons are being developed. Consequently, human exposure to MMWs is increasing.

Because of the high water content in biological tissues, MMW radiation inevitably causes sample heating due to absorption (1). Unsurprisingly, most studies into the effects of MMW exposure on biological tissues conclude that the observed impacts are strictly thermal in nature (2–4). The primary organ that absorbs most of the energy at these frequencies is the skin. Despite that the specific absorption rate and power density are maximum at the epidermis, up to 60% of the energy reaches the dermis (where nerve endings lie), and ~10% gets to the subcutaneous hypodermis (5). Early studies concluded that MMW radiation has no detectable pathological impact on skin cells and does not cause carcinogenic or other potential long-term effects (2,6–8). Nevertheless, at least one study concluded that ~5% of the observed long-term exposure effects of MMWs is caused by the EM field interaction with the tissue and not just the thermal impact (9).

A few studies have looked at the effect of MMW radiation on free nerve endings located in the skin as well as on sensory neurons and especially NIs (10–12). In one report (10), the thermal pain threshold upon skin heating with intense MMW radiation (94 GHz, 1.8 W/cm^2) was ~44°C, which is close to the normal physiological value. In contrast, comparatively low intensity MMW exposure (up to only 14 mW/cm^2) with little ensuing tissue heating was reported to have an analgesic/hypoalgesic effect (11,12). These two examples point to the complexity of the mechanisms underlying MMW interactions with tissue and the various effects they have at different levels of exposure.

Retzius neurons of the medicinal leech are naturally active with an approximate action potential (AP) firing rate of 1 Hz; previous studies found clear changes in their spiking activity when they were exposed to very low power MMWs (<1 mW/cm^2) (13–16). In addition, when the MMW irradiation of neurons was compared to thermal heating with a similar but small temperature rise (<1°C), the MMWs caused a reduction of one third in the AP firing

Submitted November 27, 2018, and accepted for publication April 15, 2019.
*Correspondence: sergii.romanenko@uwa.edu.au
Editor: Andrew Plested.
https://doi.org/10.1016/j.bpj.2019.04.021

rate (12), whereas thermal heating led to an enhancement of neuronal activity (increased firing rate by two to three times) (14). In both cases, the rising and decaying phases of the AP shortened; however, with MMW radiation, the decrease was ~10% (with respect to the initial value), whereas for thermal heating, the change averaged to ~5% (13–15,17,18).

In this article, we extend these earlier studies by examining the direct effect of higher MMW power (at 60 GHz, >100 mW/cm^2) but this time on sensory neurons from the medicinal leech (i.e., neurons that are only active when exposed to noxious stimuli, such as pressure, chemical, osmotic, and, most important for our study, temperature changes). Here, we focus on the thermosensitive nociceptor (NI), which has a step-like activation when exposed to thermal stimuli (i.e., they start firing when they are exposed to a particular temperature). The NI thermal sensitivity is attributed to the presence of transient receptor potential vanilloid 1 (TRPV1)-like capsaicin receptors (19). It is well known that TRPV1 are polymodal ionotropic receptors and, in mammalian cells, activate at a thermal threshold in the range of 42–45°C (20–23). Considering this, the null hypothesis is that MMW irradiation would induce heating that would cause the same activation of thermosensitive NI as thermal heating. The goal of this work was to determine the effects of MMW radiation on primary NIs and whether they can be accurately modeled.

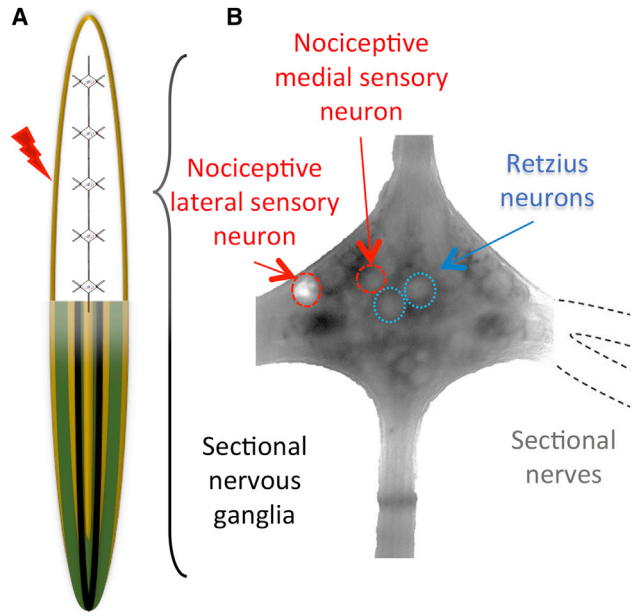

FIGURE 1 Schematic representation of pain transduction in the leech. (*A*) Shown is a schematic representation of leech body (*lower part*) and leech segmental nervous system (*upper part*). Application of suprathreshold thermal stimulus (*dark red flash arrow*) to the body wall causes the activation of the N lateral primary nociceptive neuron. (*B*) Photograph of single sectional ganglia with lateral nerves (*dashed line*) and intersectional axonal bundles is shown. Nociceptive neurons are depicted by red (*dark*) dashed circles. Retzius neurons are depicted by blue (*light*) dotted circles. To see this figure in color, go online.

MATERIALS AND METHODS

Biological model

The experimental model used here was the leech thermosensitive NI (lateral–NI); these are sensory receptors in somatic structures that convey nociceptive (pain) information to the central nervous system. The leech nociceptive receptors are remarkably similar to vertebrate NI (24) and provide numerous experimental, procedural advantages. Fig. 1 shows the relevant details of NIs and the section of leech (ganglia) studied. An advantage of this model is the ability to study individual NIs within a whole intact neuronal ganglion, which preserves interactions with other neurons and surrounding glial cells, giving a more representative "whole organ" response (Fig. S1).

Adult medicinal leeches, genus *Richardsonianus Australis*, were obtained from the Genki Centre (Glebe, NSW, AU). We have assumed that because of the similarities in size, habitat, and living conditions of the Australian leech, its physiology is essentially the same as, for example, the North American leech, which was used in previous studies. The leeches were kept in a glass aquarium with artificial pond water (36 mg/L Instant Ocean salts; Aquarium Systems, Mentor, OH) in a temperature-controlled room at 18°C and with a 12 h light/dark cycle. At the time of the experiments, leeches weighed between 1 and 3 g. Before dissection, the leech was anesthetized in ice-cold leech saline containing 115 NaCl, 4 KCl, 1.8 $CaCl_2$, 1.5 $MgCl_2$, 10 HEPES, and 10 glucose (pH = 7.35), all values in mM (reagents from Sigma-Aldrich, St. Louis, MO). Individual ganglia were dissected from midbody segments (M6–M12) and pinned down in a Sylgard184 (Dow Corning, Midland, MI)-filled dissection box. Dissected ganglia (Fig. 1 *B*) were transferred to a Petri dish (diameter: 35 mm) and pinned down (ventral side up) on a paraffin bed (Fig. 2 *B*) with four tungsten pins. Between experiments, the ganglion was maintained at an ambient temperature of 21–25°C. In experiments with a selective TRPV1 antagonist, *N*-(3-Methoxyphenyl)-4-chlorocinnamide (SB366791; Sigma-Aldrich), the stock compound (0.1 M in dimethyl sulfoxide stored at −20°C) was diluted in modified (Ca-free) leech saline to make a 50 μM final solution.

The Petri dish with the dissected ganglion was placed on an upright microscope (Nikon Eclipse E600-FN; Nikon, Tokyo, Japan) and filled with leech saline so that the ganglion was covered by about a 1-mm thick layer of fluid. The total volume of saline used was 3 mL. For proper illumination of the ganglion during the insertion of the electrolytic probe into a specific neuron, we used a bright white light-emitting diode at a very oblique incidence angle with respect to the microscope bore (25) and a 10× Plan Fluor objective with differential interference contrast filters.

Electrophysiology

To perform the electrophysiological recordings, a sharp (<1 μm diameter) intracellular electrode was fabricated from aluminosilicate capillary glass (0.87 × 1.2 mm inner/outer diameter, AF120-87-10; Sutter Instruments, Novato, CA) using a laser micropipette puller (P-2000; Sutter Instruments). The electrodes were filled with 3 M K-acetate and 20 mM KCl unbuffered solution. Average resistance was in the range of 24–27 MΩ. All electrophysiological recordings were performed using a microelectrode amplifier (Axoclamp 900 A; Molecular Devices, Sunnyvale, CA) in the current-clamp mode, held at 0 nA. Recordings were then digitized at 100 kHz using data acquisition hardware (DigiData 1550 A; Molecular Devices) and custom software (Clampex 10; Molecular Devices). Electrophysiological recordings were performed using the "gap-free" mode and episodic stimulation and were processed using Molecular Devices Clampfit 10 software. Only data corresponding to a rising temperature phase was used in the analysis. For thermal heating of the sample, a 68 W 40 × 40 mm Thermoelectric (Peltier) Module (TEC1-12708/ZP9104; Jaycar Electronics, Sydney, NSW,

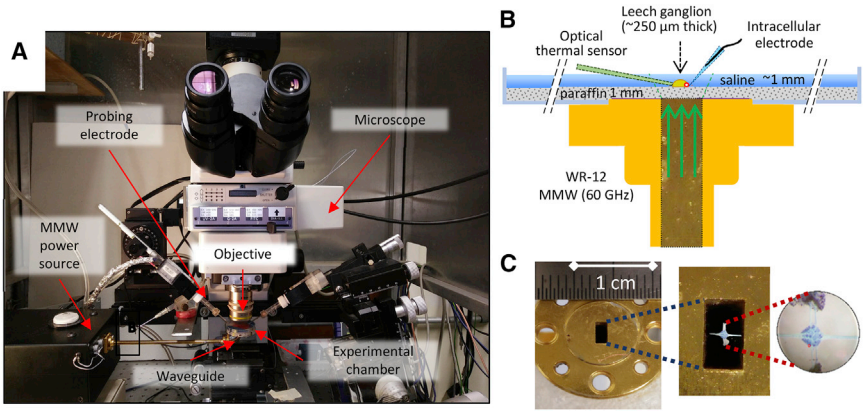

FIGURE 2 The experimental setup, leech ganglia preparation, and experimental chamber is shown. (*A*) A photograph of experimental setup is shown. (*B*) Side view schematic of the experimental setup with chamber installed on the WR-12 waveguide is shown; the ganglia is mechanically fixed with fine tungsten pins on the paraffin pad (on the picture, the ganglia size is exaggerated for the convenience of the reader). The neuron of interest was probed with a glass microelectrode; a second auxiliary glass electrode was installed as close as possible to the first one and was used for the compensation of thermal- and convection-related artifacts. The reference electrode was mounted on the edge of the chamber to avoid interference with the MMW radiation. The thermal sensor was placed as close as possible to the ganglia, perpendicular to the probing electrode. (*C*) Shown is a photograph of WR-12 waveguide top view (*leftmost picture*) with enlarged picture of its aperture overlapped with a picture of the leech ganglia (*middle picture*) and enlarged photograph of the ganglia (*rightmost picture*) stained with 1% trypan blue, fixed in cold 4% paraformaldehyde and 0.1 M phosphate buffer (pH 7.4), and washed in PBS. The circle indicates the position of one N lateral (Nl) thermosensitive nociceptor neuron. To see this figure in color, go online.

AU) was used. The sample dish was placed on top of the heating module. To separate the ganglion from the hot plate, a 2-mm thick paraffin layer was spread across the bottom of the sample. The ganglia were stretched out and pinned directly to the paraffin. For the MMW irradiation, the power was delivered directly to the cells from below (see MMW setup shown in Fig. 2 *B*). Because of the limited MMW power available, the heating rate was generally slower than for thermal heating. Hence, the average heating duration was 47 ± 10 s for thermal heating and 75 ± 13 s for MMW heating. Nevertheless, the difference in the heating rate was not considered detrimental to the experimental outcome or conclusions of this study (26). This is because activation of the thermosensitive NI is triggered only when the noxious temperature threshold is reached; all samples were heated to activation, and a continuous train of APs was recorded.

The temperature of the saline in the thermal heating experiments was monitored with a type K thermocouple having an accuracy of 0.1°C (QM1283; Jaycar Electronics). To avoid any influence the MMWs might have on the temperature measurement, a gallium arsenide crystal-based fiber-optic thermometer with a resolution 0.01°C (OTG-M280 sensor with PicoM spectrophotometer PCM-G1-10-100ST-L; Opsens, Québec, Canada) was used for all the MMW experiments; the equivalence between the two methods of recording temperature was confirmed (with an accuracy of 0.1°C).

MMW setup

The MMW exposure system consisted of a tunable microwave source from 8 to 20 GHz (yttrium iron garnet-tuned oscillator SAO 002; Virginia Diodes, Charlottesville, VA), coupled to a frequency multiplier/power amplifier chain (WR12AMC-HP; Virginia Diodes), which delivered continuous MMWs in the range 60–90 GHz with a maximal output power at any frequency of 100 mW (Fig. 2 *A*). For the neuron irradiation experiments, the system was set to 60 GHz. The MMW signal was coupled into the ganglion through a single mode open-ended rectangular waveguide (WR-12 Instrumentation Grade Straight Waveguide with UG-387/U Flange with a 3.09 × 1.54 mm aperture) placed directly under the Petri dish and encapsulated paraffin layer (Fig. 2, *B* and *C*). Using the microscope, the ganglia were aligned directly above the center of the waveguide aperture, in which the MMW field is at a maximum (Fig. 2 *C*). Note that the MMW power is incident on the ganglia after passing through the thin layer of paraffin and not through any significant amount of saline, which has a high MMW absorption coefficient (~3 cm^{-1}) (27,28). Both the paraffin and polystyrene are highly transmissive at these wavelengths (5 mm).

Cell viability experiments

The sample chamber used for the electrophysiological experiments was also used for fluorescence experiments to maintain identical environmental conditions. The Nikon Eclipse microscope was equipped with an epifluorescence attachment (Y-FL), and a high-pressure Mercury lamp (USH-102DH; Ushio Electric, Tokyo, Japan) was used for illumination. Samples were placed under the 10× Plan Fluor differential interference contrast objective, and after MMW exposure (or sham experiment), the saline in the Petri dish was quickly replaced with a PI/leech saline solution. The pinned-out ganglia were incubated for 60 s, after which fluorescence images were acquired. The PI solution was made from a stock solution (P4170, 1 mg/mL stored at −20°C; Sigma-Aldrich) by adding 1 μL stock to 1 mL of leech saline. The fluorescent images were collected by a digital charge-coupled device camera (DS-5Mc; Nikon) and stored. The resulting images were processed and analyzed with freely available ImageJ software (http://imagej.nih.gov/ij/) (29). To eliminate the stray background signal and estimate cell signal intensity above it, the measured intensities were treated as $\Delta I/I = (I_G - I_{BG})/I_{BG}$, where I_G is the signal from ganglia, and I_{BG} is the signal from background.

Dosimetry and radiation exposure simulations

The attenuation of MMW power from the exit port of the waveguide to the ganglion was measured using a pyroelectric detector system equipped with a broadband Winston cone (multimode power collecting funnel) and an infrared-blocking filter (DLA-TGS with a 6 THz low-pass edge filter; QMC Instruments, Cardiff, UK). With no saline present, the attenuation of the MMW power through to the top of the paraffin was 43%, with respect to the power at the waveguide output. When the full 3 mL of saline was added to the Petri dish (to a level 1 mm above the paraffin), the MMW signal was reduced by 31 dB (<1/1000th of the power at the waveguide output) because of the absorption by the aqueous solution.

To estimate the MMW power density across the ganglion, one must know both the absorption and reflection coefficients of the intervening layers between the ganglion and the waveguide aperture as well as the radiation divergence that occurs as the MMW energy exits the waveguide aperture and is then refracted at each intervening surface. This had to be estimated using an electromagnetic (EM) model of the experimental setup because the pyroelectric detector was not able to probe the MMW fields at the length scale of the ganglia (generally smaller than one wavelength). A commercial EM simulator based on finite difference time domain (QuickWave; QWED,

Warsaw, Poland) (14,15) was employed. Distribution of the MMW power density along the vertical axis, and at selected horizontal cross sections, were estimated from an EM simulation of the exact layout of the waveguide and Petri dish at 60 GHz. The EM simulator requires prior knowledge of the relative permittivity ε_r and conductivity σ of all materials encountered. Values for the leech saline solution, the paraffin, and the polystyrene Petri dish were measured using a commercial THz time-domain spectroscopy system (TeraPulse 4000; TeraView, Cambridge, UK) over the temperature range used in the experiments (24–45°C). At ambient temperature, the measurements yielded the following: saline $\varepsilon_r = 12.01$, $\sigma = 72.64$; the paraffin layer $\varepsilon_r = 2.27$, $\sigma = 0.02$; and polystyrene $\varepsilon_r = 2.56$, $\sigma = 0.09$ (Fig. S2). The properties of the saline increase linearly with the temperature as expected for aqueous solutions (30), and this data was also used in the biophysical simulations. For the leech ganglion (0.2-mm thick), the dielectric constant and conductivity were estimated to be the same as those measured brain tissue samples in the literature (31) of $\varepsilon_r = 10.9$ and $\sigma = 48.5$ were employed for the EM simulations.

EM simulations were performed at 60 GHz with 100 mW of continuous wave power exiting the waveguide aperture. The calculated power density distributions at various positions along the path from waveguide aperture to ganglion are shown in Fig. 3. The power density varies across the waveguide aperture as shown in the cross section and is 470 mW/cm^2 at the center of the guide. Beam expansion modified by refraction and reflection at each surface and absorption within each dielectric layer accounts for a difference in the power density of ~17% from the waveguide aperture to the top of the ganglion. Accordingly, the power density at the top center of the ganglion was 82 mW/cm^2, whereas at the bottom it was 170 mW/cm^2; therefore, we assume that ~50% of the incident power is absorbed in the ganglion. Note that the power distributed across the diameter of the ganglion is uniform so that any neuron that is probed in the actual experiment receives the same MMW energy and has the same specific absorption rate. Also note that the saline surrounding the sides and above the top of the ganglion absorbs all the remaining incident MMW energy so that reflections from the top of the saline layer can be ignored (32,33).

Biophysical simulations

Simulations of the electrical activity of the leech lateral N-cell (Nl) were performed with NEURON Simulation Environment (version 7.4; Hines, Yale University, New Haven, CT) (34–36). The neuron model was inspired by the work of Nicholls and Baylor (37) and was modified from Baccus (38) and includes voltage-gated sodium tetrodotoxin-resistant (I_{NaTTXR}) and tetrodotoxin-sensitive channels (I_{NaTTXs}); potassium delayed rectifier (I_{Kk}) and potassium transient current (I_A) channels; calcium current channels (L type-like); calcium-dependent potassium current channels (I_{KCa}); Na/K–ATPase ($I_{Na/K\text{-}ATP}$); leakage current (I_L); mechanisms for intracellular calcium and sodium accumulation (Ca–accum, Na -accum); and the plasma membrane Ca^{2+} ATPase (PMCA–Ca-pump) and thermosensitive receptor–vanilloid receptor type 1–TRPV1 channel. The model formulations are available at http://senselab.med.yale.edu/ModelDB/showModel.cshtml?model=236323.

The modeling of the Gouy-Chapman-Stern potentials and ion distribution nearby and on the neuronal membrane surface was performed using formulations provided by (39) and (40). The model was modified to take into account the temperature dependence of the ion hydrated radii (41) and a concentration-dependent component adapted from Stogryn (42). It also includes the thermal dependence of the leech saline dielectric permittivity as described in Dosimetry and radiation exposure simulations.

Data processing and statistics

The data were analyzed using the statistical packages in Origin2018 (OriginLab, Northampton, MA) and MATLAB 2015 (The MathWorks, Natick, MA). Data retrieved from the gap-free electrophysiological recording mode were processed with a modified MATLAB code (43) that includes the methods of (44). The AP activation threshold (V_{th}) is a threshold value of transmembrane potential, after which AP is formed in accordance with the "All or None" principle. As stated in (44), "the AP threshold is a quantifiable feature correlated to a neuron's propensity to fire an AP." V_{th} was calculated using the Maximal Slope method, which "defines V_{th} as the voltage corresponding to a maximal increase in a change in inward current relative to V (membrane potential)" (44). Specifically, $V_{th} = \max\left[g\left(t, V, \frac{dV}{dt} > 0\right) > 0\right]$, *where* $g = \frac{d^2V/dt^2}{dV/dt}$. The method was used after the resting potential baseline was subtracted from the recorded electrophysiological trace. All codes are available on GitHub (45).

The normality of the data sets was evaluated using the Kolmogorov-Smirnov test (and additionally by Anderson-Darling and Shapiro-Wilk tests) and a graphical method in *Q-Q plot* (provided in the Supporting Materials and Methods). For normally distributed data, a one-way analysis of variance (ANOVA) analysis was applied, followed by one-sided post hoc Holm-Bonferroni and Tukey's *t*-tests. For non-normally distributed data (rejection by normality test), the nonparametric Kruskal–Wallis test (KW-ANOVA) was used with data median and the *p* value provided in the text for every case. Significance levels of $p < 0.05$ were used (unless otherwise specified). The results are reported as mean ± SE (unless otherwise specified). Where used, the goodness of fit was reported as reduced χ^2 and adjusted coefficient of determination ($\bar{R}^2$).

To evaluate how the triggered AP trains correlate with temperature of the sample, characteristic AP parameters such as amplitude – the maximal depolarization value, AP half-width – the AP width on the level of half amplitude, AP maximal rise rate (MaxRise) – *max(dV/dt > 0)*, and AP maximal decay times (MaxDecay) – *max(dV/dt < 0)* were evaluated and analyzed against the temperature. Correlation analysis (Pearson correlation coefficient) was performed using standard MATLAB functions within the developed code (available in the same GitHub repository) and Origin 2018.

RESULTS AND DISCUSSION

Vitality test

To confirm that the highest intensity MMW exposures did not cause damage to neurons in the ganglia, a viability test was conducted. We used propidium iodide (PI), a DNA-binding stain, which does not enter healthy neurons but passes through the membrane of damaged cells. We used our standard experimental arrangement with saline surrounding the ganglia. The samples (n = 11) were heated, using the thermoelectric module, from a starting temperature of 22–25°C to a final temperature of 38–40°C. After the bath temperature reached its maximal value, the ganglia were kept exposed to MMW radiation for 5 min using 100 mW at the waveguide port and ~170 mW/cm^2 at the bottom of the ganglia. At the end of the exposures, the saline in the measurement chamber was replaced with a PI solution at 22–25°C. Fluorescent images of ganglia were taken within 1 min of the MMW exposure, and luminescence was measured with a photometer in the microscope eyepiece. The samples exposed for 5 min showed no difference from the control (ΔI/I for MMW versus Sham exposure is 0.18 ± 0.05 and 0.22 ± 0.03, n = 5 vs. n = 7, one-way ANOVA with Fisher test means comparison $p = 0.68$). However, the samples exposed for more than 15 min (ΔI/I = 0.67 ± 0.11, n = 6, $p < 0.01$) had a

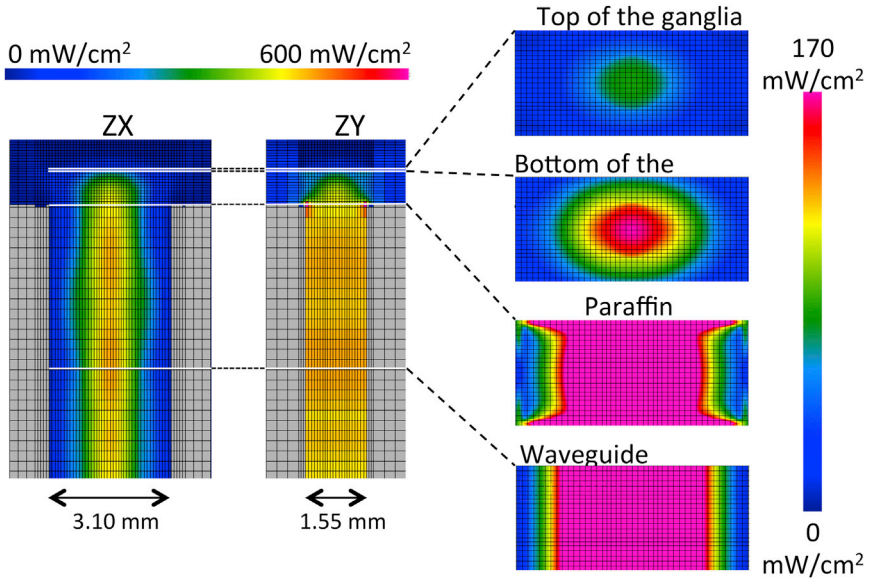

FIGURE 3 Finite difference time domain simulation of the MMW power distribution in the experimental setup. Shown is the power distribution throughout from the waveguide and through chamber in ZX and ZY projections (*left*) and power distribution on the different XY levels of the model (*right*). The power density estimated at the bottom of the ganglia was 170 mW/cm^2 and at the top was 85 mW/cm^2. To see this figure in color, go online.

noticeable accumulation of PI in the neurons and the microglial cells located on the surface of the ganglionic sheath. The estimated median lethal dose calculated from these data is 8.21 min. We therefore concluded that for heating and exposure times below 5 min, there was no evidence of cell death, and most of the experiments were conducted in less than 3 min.

Electrophysiological responses of Nl neurons exposed to MMWs compared to thermal heating of the bath

AP voltage threshold

The major thrust of this work was to determine the impact of MMW exposure compared to thermal heating on sensory neurons, specifically on the voltage activation threshold. We used a standard Axoclamp 900A and K-acetate-filled pulled capillary microelectrodes to probe changes in the electrical activity of Nl neurons in the medicinal leech.

Example recordings over 18 s from MMW and thermal exposure experiments are shown in Fig. 4, *A* and *B*, respectively. The corresponding temperature recordings measured near the ganglia are shown in Fig. 4, *C* and *D*, noting that both start at ~30°C. Generally, the Nl neurons have a high-threshold AP and rarely generate spikes when below the thermal threshold; therefore, no spikes are seen in the first part of the traces (Fig. 4, *A* and *B*). Once activated by a thermal stimulus, they generate a continuous AP train as long as the stimulus is present. For the MMW trace (Fig. 4 *A*), this occurs around 7 s when the temperature reaches 35°C; for the thermal trace (Fig. 4 *B*), this occurs around 13 s when the temperature hits 40°C. Over all experiments, the average threshold temperature (here estimated from first five APs only) was lower for MMW radiation 34.9 ± 0.4°C compared with thermal heating, which was 36.6 ± 0.4°C (KWANOVA comparison of MMW and thermal heating medians: 34.6 and 36.1°C, respectively; $\chi 2 = 9.7, p < 0.05$) (Fig. S3). Fig. 4 *F* shows the probability of the AP formation with temperature, and there is heavy overlap between the MMW and thermal groups. Because of the size and location of the temperature probe, we are not certain that the temperature of the neuron within the focal region of the MMWs was at a higher temperature than measured. In all our experiments, both thermal heating and MMW irradiation activated Nl neurons and caused the formation of AP trains, which were recorded for an average of 61 ± 16 s. When taking all APs recorded into consideration, the median activation temperature was between 39 and 40°C. Because Nl neuron thermal activation is a threshold-based mechanism, the heating rate was irrelevant (26).

The examples traces in Fig. 4, *A* and *B* also show that the pattern of response of thermal and MMWs was not identical (i.e., the spiking rate at the time of the AP train initiation and its change during the heating process); this was true for all recordings. Thermal heating evoked dense AP trains with a high initial AP spiking rate (Fig. 4 *B*, 13–18 s) when compared to MMW irradiation (Fig. 4 *A*, 7–18 s). However, we should note that the average rate of temperature rise was different; for MMW, it was 0.11 ± 0.02 and 0.27 ± 0.10°C/s for thermal heating. However, we should also note that the spiking rate in the case of thermal heating continues to increase with temperature, (Fig. 4 *E*, *red dash-dot curve*) peaking at ~9 Hz; contrastingly, the spiking rate for MMWs (Fig. 4 *E*, *green dashed curve*) peaked at the activation temperature at ~3 Hz but then dropped to a steady ~1 Hz.

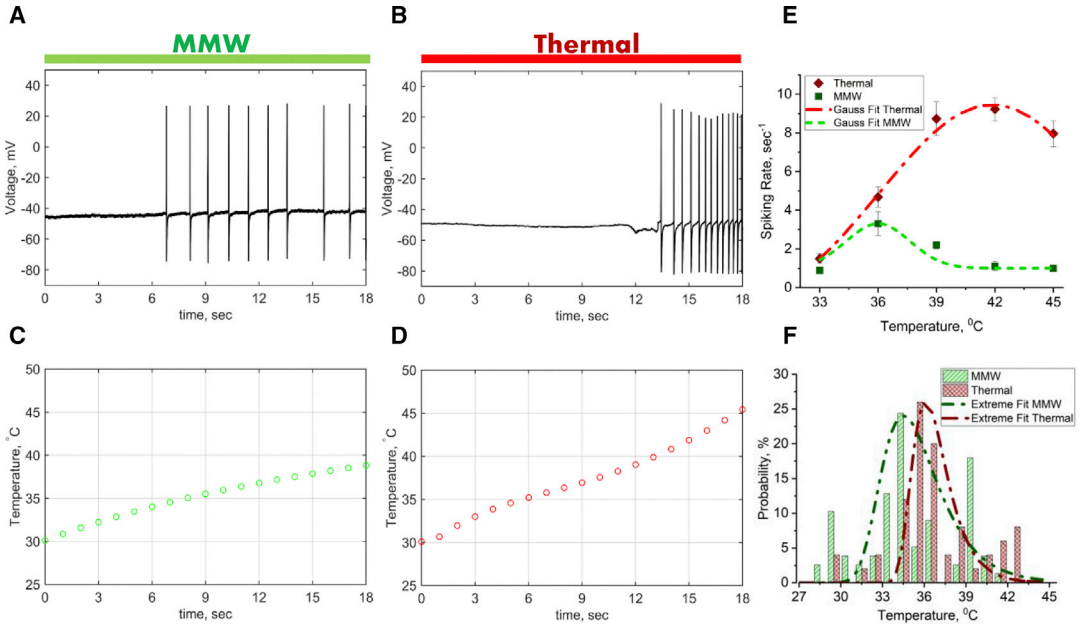

FIGURE 4 This shows the effect of MMW and thermal heating on Nl neurons. (*A*) is a representative recording of Nl neuron activation using MMW irradiation. Upper trace (*A*) is the transmembrane voltage recording from Nl soma, and lower trace (*C*) is the temperature of the saline adjacent to the ganglia. (*B* and *D*) The representative recordings of Nl neuron activation by thermal heating. (*B*) is the transmembrane voltage, and (*D*) is the temperature. (*A*) and (*B*) demonstrate a typical electrophysiological reaction of the primary nociceptive neurons to a temperature change from 30 to 38–45°C. In both cases (MMW and thermal heating), Nl neurons remain "silent" up until a threshold temperature is reached, after which the AP train is generated. Although the activation of Nl neurons is a threshold-based process, the AP spiking rate change is a process gradually evolving with sample heating. (*E*) The change of AP spiking rate along with the time for traces subjected to MMW radiation (*green square marker*) and thermal heating of the saline (*red diamond marker*) is shown. The data binned every 3°C and were represented as mean ± SE. Data are fitted with Gaussian curve: for MMW (*green dashed line*; $\bar{R}^2 = 0.44$) and thermal heating (*dot-dashed line*; $\bar{R}^2 = 0.99$). (*F*) Shown is the probability distribution of first five AP against temperature in NI neurons caused by thermal heating (*red cross-stripped bars*) and MMW (*green slant-stripped bars*). Distributions are fitted with a skewed Gaussian; the fit for MMW is represented by a green dashed-double dot line ($\bar{R}^2 = 0.98$), and thermal heating is represented by a dark-red dash-dot line ($\bar{R}^2 = 0.66$). To see this figure in color, go online.

For some experiments, we continued to record the APs when the MMWs or the thermoelectric module was switched off. The return of the neuron to its initial nonexcited state is different between MMW and thermal heating (Fig. S4). The AP firing for the MMW exposure ceased quickly after the source is switched off, even though the bath temperature is still above the activation threshold (observed in 100% (12/12) of recording in which APs were measured during heating and cooling). Whereas for the NI neurons exposed to thermal heating, once switched off, the AP firing continues even though the bath temperature falls well below the original threshold (observed in 90% (9/10) of recordings).

We tested the correlation of temperature and several AP parameters (amplitude, AP half-width, MaxRise, MaxDecay) for both MMW irradiation and thermal heating over the range 36–46°C, and no correlations ($R^2 > 0.5$) were found.

We defined an activation voltage threshold if at least five AP signals are generated in a train. The results are summarized in Fig. 5. The mean voltage threshold of AP activation for thermal heating was 8.3 ± 0.4 mV (n = 20), whereas for MMW exposure, it was 3.9 ± 0.4 mV (n = 16) (KWANOVA comparison of thermal heating and MMW medians: 8.2 and 3.0 mV, respectively; $\chi 2 = 58$, $p < 0.01$). The comparison of AP voltage threshold distribution (throughout the entire range of observed temperatures) from MMW and thermal heating experiments revealed different ranges of voltage threshold deviation. For thermal heating, activation varied from 0.5 to 16 mV, whereas for MMW, it was 0.5–8.5 mV (Fig. 5, *B* and *C*). Also, it can be seen in the same figure that from cumulative frequency curves, thermal heating has a broad distribution range, whereas MMW demonstrates a single distribution curve (low voltage thresholds) within a narrow distribution range. At this point, we do not have a good physiological model for this behavior. However, others have noted similar enhanced AP firing due to activation and inactivation kinetics of ion channels, conduction velocity, and synaptic events among other phenomena (46–48).

In summary, the most important finding was that neurons subjected to the MMW radiation have an activation voltage threshold for AP formation half of that compared to thermal heating.

AP current threshold

In addition to the experiments on AP voltage threshold and changes in AP magnitude and shape characteristics, we

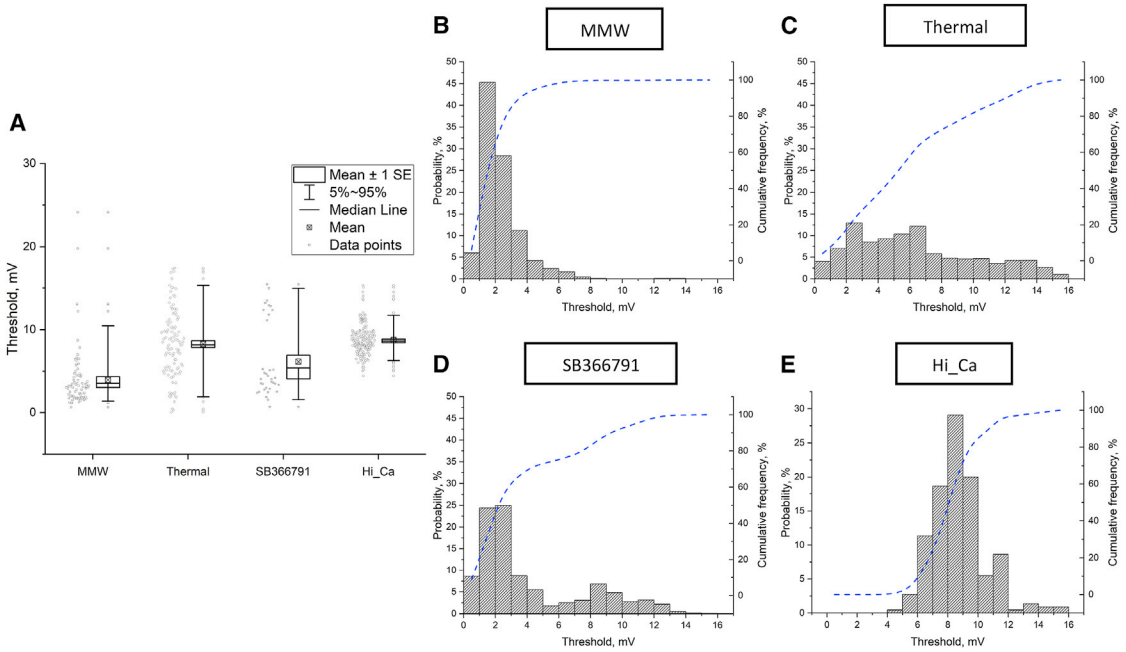

FIGURE 5 The effect of thermal and MMW heating on Nl neuron activation threshold. (*A*) The Nl neuron voltage thresholds averaged over the first five AP in a train under the condition of MMW exposure (n = 16) and thermal heating (Therm.Heat, n = 20), MMW irradiation on cells treated with TRPV1 antagonist (SB366791, n = 7), and cells incubated in "high-Ca" saline (normal concentration ×5 = 9 mM, n = 7). Only one AP train per cell was analyzed. Data are mean ± SE; median and 5–95% range are shown along with the scatter plot of individual data points. Group comparison with KWANOVA is shown ($\chi 2(3) = 130.23$, $p < 0.05$); (*B–E*) shown is the voltage threshold probability distribution (*bar plot*) and cumulative frequency (*dashed line*) of all AP in trace of all recorded traces (one trace per cell) for MMW ((*B*) details in AP voltage threshold), thermal heating ((*C*) details in AP voltage threshold), MMW plus SB366791 ((*D*) details in The effect of MMW irradiation in the presence of TRPV1 antagonist), and MMW plus "high-Ca" ((*E*) details in The effect of MMW in the presence of a high concentration of divalent cations). To see this figure in color, go online.

looked at neuron excitability under control conditions and MMW exposure. Because activation of Nl neurons by MMW radiation generated AP trains at a lower voltage threshold, it was necessary to test how MMW radiation can influence the voltage-gated conductivities of the neurons. To avoid the involvement of TRPV1-like channel activation, the test was conducted at room temperature with short MMW pulses. We employed a current-clamp step protocol to investigate potential alterations in the current threshold of AP formation in Nl neurons under control and test conditions. Current steps (10 ms) were delivered in a current-clamp mode at room temperature. In test experiments with MMW radiation, the neurons were exposed for 500 ms (during −0.25 nA hyperpolarizing pulse) before the depolarizing current step was applied (Fig. 6 *A*). The short time for the MMW exposure ensured that temperature changes were minimal (0.27 ± 0.02°C). The magnitude of the current step that triggers AP formation was considered as a current threshold. The comparison of control and MMW test demonstrated that application of MMW did not increase Nl neuron excitability (Fig. 6 *B*). The threshold current in control conditions (0.79 ± 0.07 nA, n = 7) was not different to the MMW test (0.68 ± 0.13 nA, n = 8, one-way ANOVA, $p = 0.46$). Utilization of current step protocol under conditions similar to AP voltage threshold did not reveal a statistically significant difference between the control and MMW data (Fig. S5). This result demonstrates that voltage-gated conductivities in Nl neuron do not have specific or significant sensitivity to MMW radiation.

Passive parameters

To estimate the contribution from passive electrophysiological properties of the probed neuron, we injected negative current pulses that resulted in no AP generation. We then measured the capacitance and conductance under MMW and thermal heating over the range of 34–39°C versus the control of 20–22°C. In the case of MMW irradiation, the mean electrical resistance was significantly higher with a value of 68.3 ± 4.1 mΩ than both the control and thermal heating, which were 47.5 ± 1.7 mΩ and 52.1 ± 1.9 mΩ, respectively (n = 9; KWANOVA medians comparison: 49.5 vs. 38.7 and 47.2 mΩ, correspondingly; $\chi 2 = 13.3$, $p < 0.01$). The capacitance, however, had a somewhat lower value for the MMW-exposed samples (9.7 ± 4 pF) than either the control or the thermally heated neurons (14 ± 1 and 12 ± 2 pF, respectively), although the differences in the three values are not significant when taking the errors into consideration. These results show that passive physiological parameters do not change significantly with thermal heating below threshold temperatures, whereas altered resistance under MMW exposure does not contribute to the sensitization we have observed.

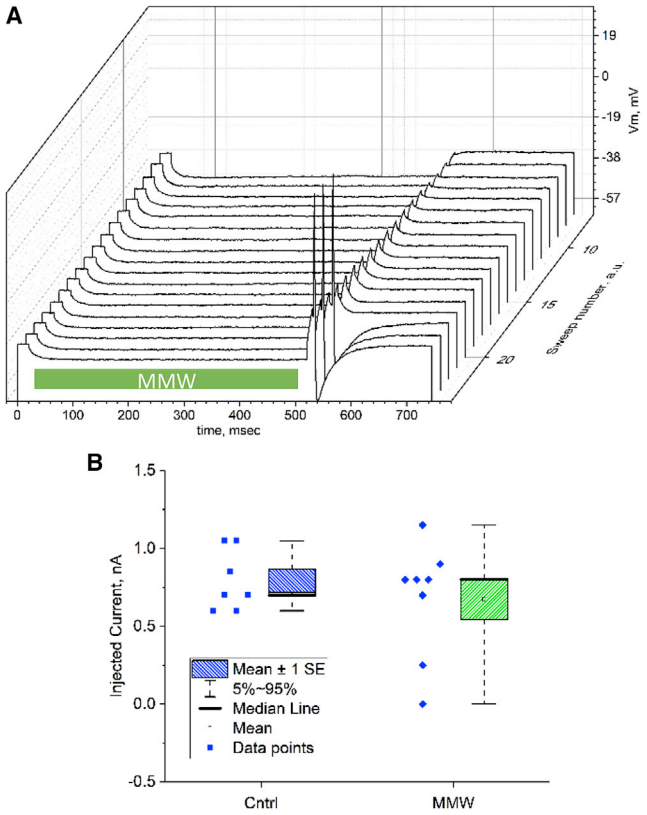

FIGURE 6 The effect of MMW radiation on injected current pulse activation threshold in Nl neurons at room temperature. (*A*) Representative recordings of cell response to current step protocol are shown. When a critical (threshold) current pulse is applied, the Nl neuron generates AP. The duration of stimulatory pulse of 10 ms, and the current increment is 0.05 nA. Stimulatory pulse was preceded by 500 ms and −0.25 nA hyperpolarizing pulse. The horizontal (*green*) bar indicates the time of MMW application. (*B*) The pulse current activation thresholds were measured in control conditions and MMW test. Data are mean ± SE; median and 5–95% range are shown along with the scatter plot of individual data points. Group comparison with ANOVA is shown (Cntrl. −0.8 ± 0.1 nA, n = 7; MMW test 0.7 ± 0.1 nA, n = 8, one-way ANOVA, $p = 0.46$). To see this figure in color, go online.

Multimodality of MMW effect

The effect of MMW irradiation in the presence of TRPV1 antagonist

As noted in the current step experiments (Electrophysiology), thermal activation by MMW irradiation is not based on changes to the AP driving conductance. However, further work was needed to clarify whether changes to thermally sensitive TRPV1 are the basis for the observed lower voltage thresholds upon MMW exposure. We used a selective cinnamide TRPV1 antagonist (SB366791) to see if this would reduce or eliminate the threshold effects seen under MMW irradiation (49). It is known that this antagonist does not interfere with voltage-gated calcium channels and with hyperpolarization-activated channels (unlike Capsazepine), and it blocks thermal and capsaicin-evoked responses in leech Nl neurons (19). For these experiments, the ganglia were incubated in 50 μM of antagonist for 5 min before being exposed to the MMW irradiation (170 mW/cm^2 for less than 3 min), and the heating of the bath was limited to 44–45°C.

Taking the full suite of temperature-dependent data and comparing the change in the AP activation threshold (estimated from first five AP) yields a significant difference between the neurons in the antagonist and normal saline solutions (Fig. 5 *A*): 6.2 ± 0.8 mV (n = 7) vs. 3.9 ± 0.4 mV (n = 16) (KWANOVA medians comparison: 4.1 and 3.0 mV, correspondingly; $\chi 2 = 9.2$, $p < 0.05$). Also, the neurons in the antagonist solution have an AP voltage threshold probability distribution (Fig. 5 *D*) that is very similar to that obtained from the thermal heating experiments (AP voltage threshold)—i.e., have a wide range of voltage thresholds (0.5–11 mV) and could be represented by bimodal distribution of high and low voltage thresholds. Nevertheless, the presence of antagonist in the bath solution did increase the probability of AP with a lower voltage threshold. Hence, the effect of MMW irradiation on Nl neurons could be the result of either multimodal facilitated activation of TRPV1 (simultaneous thermal and osmotic) or activation of another sensory channel in the neuron's membrane (see below).

The effect of MMW in the N-medial neurons

It is reasonable to assume that Nl neuron osmosensitivity could be due to the activation of another channel. Indeed, another member of the transient receptor potential vanilloid family, namely TRPV4, is a known osmosensitive channel that responds to mechanical stimulation (50,51). Thus, we cannot exclude the possibility that this channel or its homolog may be present in the leech neuron membrane and perform as a complementary sensor in nociception. To rule out a separate sensory channel, we tested a different type of neuron, the N-medial (Nm) neurons in the ganglia, which are mechanical NIs (52). These neurons are also high-threshold NIs and homologs of the Nl neurons (hence, it is very likely that TRPV4 can be present on the membrane of this neuron). However, they do not express sensitivity to high-temperature stimulus, nor do they respond to capsaicin. The Nm neurons were probed in the same manner as the Nl neurons, but in contrast, the introduction of the electrode results in continuous AP spiking (presumably triggered by membrane stretch around the electrode or previous Nm terminals cut off during the preparation, causing a typical response). Such spiking remained as long as the activity of neuron was observed (Fig. 7 *A*); even the injection of a prolonged hyperpolarizing current did not suppress this activity in the Nm cells. Under normal conditions (20–25°C), the mean spiking rate of Nm neurons was 2.03 ± 0.13 Hz. After MMW stimulus was applied, the spiking linearly increased with a rate of 0.17 ± 0.03 Hz/s (Fig. 7 *B*). Unlike the NI neurons, in the Nm, MMW irradiation (170 mW/cm^2) did not result in step-like alterations in neuron activity, but

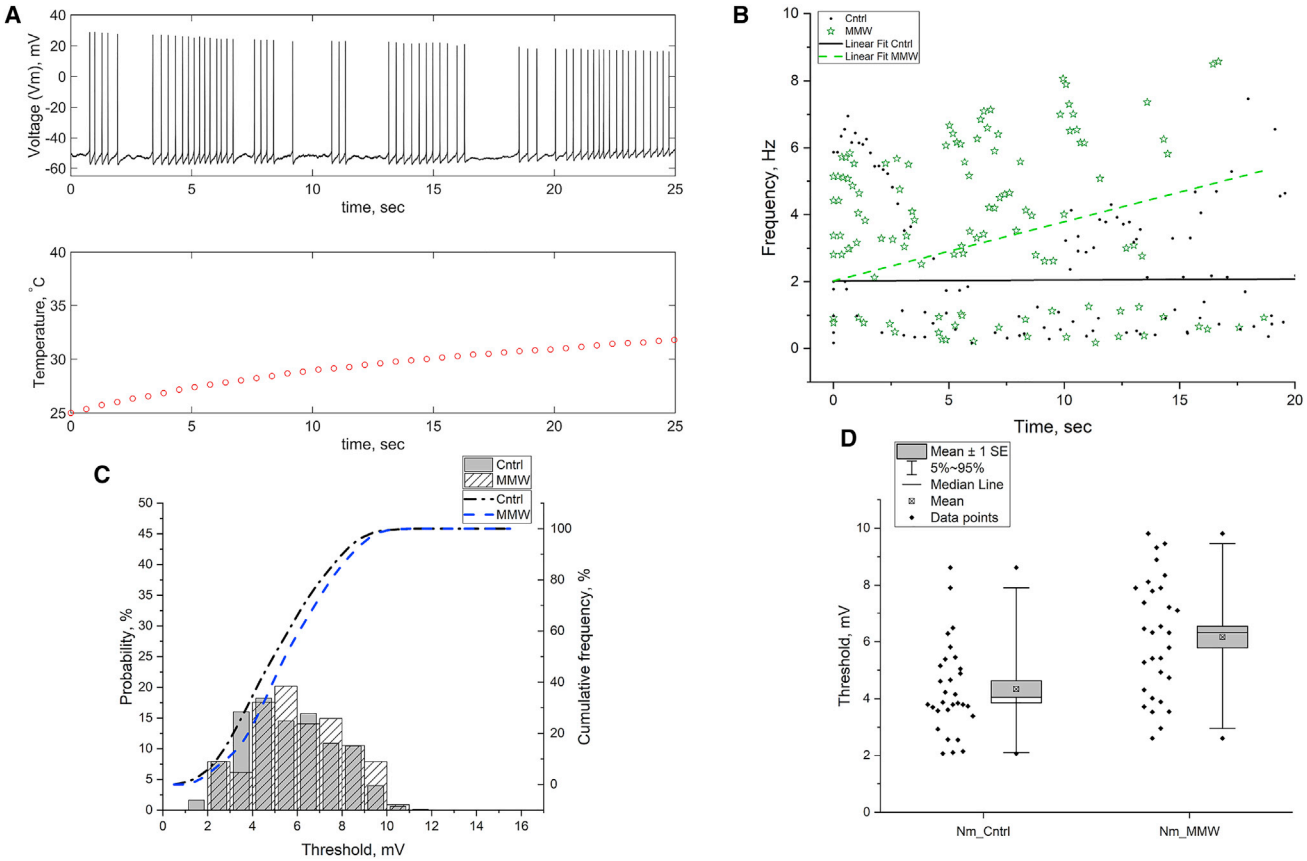

FIGURE 7 Electrophysiological characteristics of Nm neuron in control conditions and under MMW radiation. (*A*) The representative recordings of the Nm neuron electrophysiological activity alterations under MMW irradiation are shown. The upper trace is the transmembrane voltage recorded from the Nm soma, and the lower trace is the temperature of surrounding saline. (*B*) The alterations in Nm neuron AP firing frequency versus time for the control (*black dots*) and during the MMW radiation (*green stars*) are shown; solid lines are linear data fittings for pre-exposure control (*black line*) with a constant value of 2.03 ± 0.13 Hz throughout the entire range of observations and during MMW exposure (*green dashed line*), slope is 0.17 ± 0.03 Hz/s, and constant coefficient was forced into value 2.03 Hz, $\bar{R}^2 = 0.67$. (*C*) The threshold voltage probability distribution for Nm neurons before (Cntrl, *shaded bars*) and during MMW exposure (MMW, *slant-stripped bar*) and threshold voltage cumulative frequency before (Cntrl, *black dash-dot line*) and during MMW radiation (MMW, *blue dashed line*). (*D*) Shown are the voltage thresholds for five first AP recorded from Nm neurons before (Cntrl, −4.3 ± 0.3 mV) and during MMW radiation (MMW, −6.2 ± 0.4 mV). Data are mean ± SE (group comparison ANOVA $p < 0.05$); median and 5–95% range are shown along with the scatter plot of individual data points. To see this figure in color, go online.

gradual changes were observed (Fig. S6). The temperature increase caused proportional changes in the AP firing of Nm neurons (Fig. S5). Despite the spontaneous activity of Nm neurons, which means that it does not require any additional current to trigger the AP generation, the voltage threshold is still one of the main characteristics of the AP and cell activity in general. Hence, it is a useful characteristic for the comparison of neuronal reactions under different experimental conditions (44). A comparison of the first five AP voltage thresholds before and during MMW exposure showed an increase V_{th}: 4.3 ± 0.3 vs. 6.2 ± 0.4 mV (n = 6, one-way ANOVA, $p < 0.05$) (Fig. 7, *C* and *D*). Note that, here, we compare the AP thresholds from slightly different temperature ranges 22.7 ± 0.8°C for control data and 24.9 ± 1.5°C for MMW data (Fig. S5). Even though the sample was heated by MMW exposure, the AP threshold under this condition was higher than under control ones. This is consistent with the results obtained in AP current threshold and Passive parameters. Because the Nm neuron does not have the thermal sensor (TRPV1-like channel) and hence do not replicate the effect seen for Nl neurons (in AP voltage threshold), we conclude that the mechanism underlying the lower activation threshold in Nl neurons exposed to MMW radiation is due to the multi-modal activation of TRPV1 receptors.

The effect of MMW in the presence of a high concentration of divalent cations

One of the environmental modalities that could activate the TRPV1 channels and its homologs is osmolarity. Considering that one of the most abundant ions near the outer surface of the cell membrane is calcium, we assumed that triggered alteration in the concentration of this ion could be a factor that influenced TRPV1-like channel sensitization

in Nl neurons. At the same time, an increased concentration of calcium in bulk solution would buffer any fluctuations of this ion in the perimembrane space. In this case, it would be reasonable to expect that the effect of any external influence on the osmotic ion gradient near the membrane surface would be suppressed. We tested the combined effect of an increased calcium concentration in the bath solution and MMW irradiation on the Nl neurons. The experiments were conducted in the same fashion as described in AP voltage threshold. The concentration of extracellular calcium was increased by a factor of 5 ("Hi-Ca" = 1.8 × 5 = 9 mM) by adding $CaCl_2$, a concentration which would not cause an osmotic imbalance between intracellular and extracellular media in leech neurons (53). With 9 mM calcium concentration in the saline, the osmolarity changed ~7% (the variation of the physiological solution up to 10% can be considered as acceptable (54)). Also, the advantage of such an experiment is that the osmolarity of the bath solution does not change significantly, and thus, there is no direct sensitization of the TRPV1-like channel. Results of this test are presented in Fig. 5, *A* and *E*. As seen in normal saline, Nl neurons preincubated in high calcium responded to MMW radiation with an AP train. But the comparison of voltage thresholds revealed a significantly increased value for "Hi-Ca" versus MMW control (8.8 ± 0.1 mV (n = 7) vs. 3.9 ± 0.4 mV (n = 16)) and KWANOVA medians comparison (8.4 and 3.0 mV, correspondingly; $\chi 2 = 131$, $p < 0.05$). In contrast to the MMW effect in normal saline, the AP voltage threshold probability distribution and cumulative frequency (Fig. 5 *E*) for neurons incubated in high calcium solution has no low threshold component and is centered very close to the high-threshold (4.5–16 mV) component of thermal heating distribution. Thus, a high calcium concentration in the bath solution eliminates the effect of MMW sensitization of the TRPV1-like channels in Nl neurons.

Computer simulation of the Nl thermal activation

At this point, we have seen that MMW irradiation of Nl neurons results in electrophysiological changes that are different from exposure to thermal heating. Some differences are pronounced, such as changes to the voltage threshold for AP activation, and others were less significant, such as alterations in cell membrane capacitance. To understand whether MMW-mediated shifts in Nl sensitivity are a result of simple temperature dynamics or some more complex mechanism, we tested different assumptions on a computer model of the Nl neuron.

Our model was implemented in NEURON simulation environment (version 7.4; Hines, Yale University) and is based on neuron simulations such as those reported in (38) and adjusted according to (37). The model is thermally robust and reliably generates APs at simulated temperatures up to 50°C. The properties of the TRPV1 mechanism were adjusted to replicate the features of leech neurons (Supporting Materials and Methods). The simulation of the model Nl neuron activation with the thermal stimulus (thermal heating) is presented in Fig. 8 *A*. After reaching the thermal threshold, the model neuron generates a stable AP train (as observed in experiments). We tested whether the rate of the temperature rise has any impact on the simulated Nl activation threshold. A comparison of a different rate of heating −0.7 and 2.3°C/s (to reduce the simulation time, the in silico heating rates were higher than those measured in the in vitro experiments, although the ratio of the heating rates was kept the same) show no dramatic impact on the threshold in the model neuron. We also tested changes in cell capacitance. We considered that dynamic change of the neuron's capacitance should be reflected not just in the membrane parameters but as an additional current ($(dC_m/dt) \times Um$, where C_m is the membrane capacitance, and U_m is the transmembrane potential) in the AP excitation equation. The rate of capacitance change in the model is taken to be proportional to the temperature with a maximal decrease of 10% compared to the starting value. The simulations showed no significant change to Nl neuron activation with changing capacitance.

From our experiments, we hypothesize that TRPV1 channels are sensitized during MMW irradiation and that two mechanisms, thermal and osmotic activation of TRPV1, are involved. We know from the literature (55) that an increase in osmolality up to 350 mOsm causes sensitization and can even activate the TRPV1 channel. We assumed that MMW radiation promotes a local perimembrane perturbation of solute concentration. The test with high calcium concentration (×5) in bulk solution supported this assumption by eliminating the MMW effect due to the buffering of perimembrane calcium concentration fluctuations. However, the question of whether MMWs can change the perimembrane solute concentration up to 350 mOsm still remains. To address this issue, we used a Gouy-Chapman-Stern computational model (Fig. S9) of an ionic double layer on the surface of the membrane (39,40,56). The model relates the membrane surface charge with the surface potential and electrolyte concentrations. It accounts for the temperature of the system, ion hydration radii, and the temperature dependence of the saline dielectric properties. Values for the surface charge density were taken from the Hille estimation (57–59)—one electron charge per 100–400 Å. The asymmetry in charge density for inner and outer leaflets of the membrane were introduced with an outer layer having approximately three times more charge (60). The model calculates the distribution of electrostatic potential and electrolyte concentration within membrane surface proximity. We ran the simulation for different temperatures within our experimental range. Even with a change in temperature of 20°C, the surface potential altered by just a few millivolts. Even smaller changes occur for the perimembrane concentration of the sodium

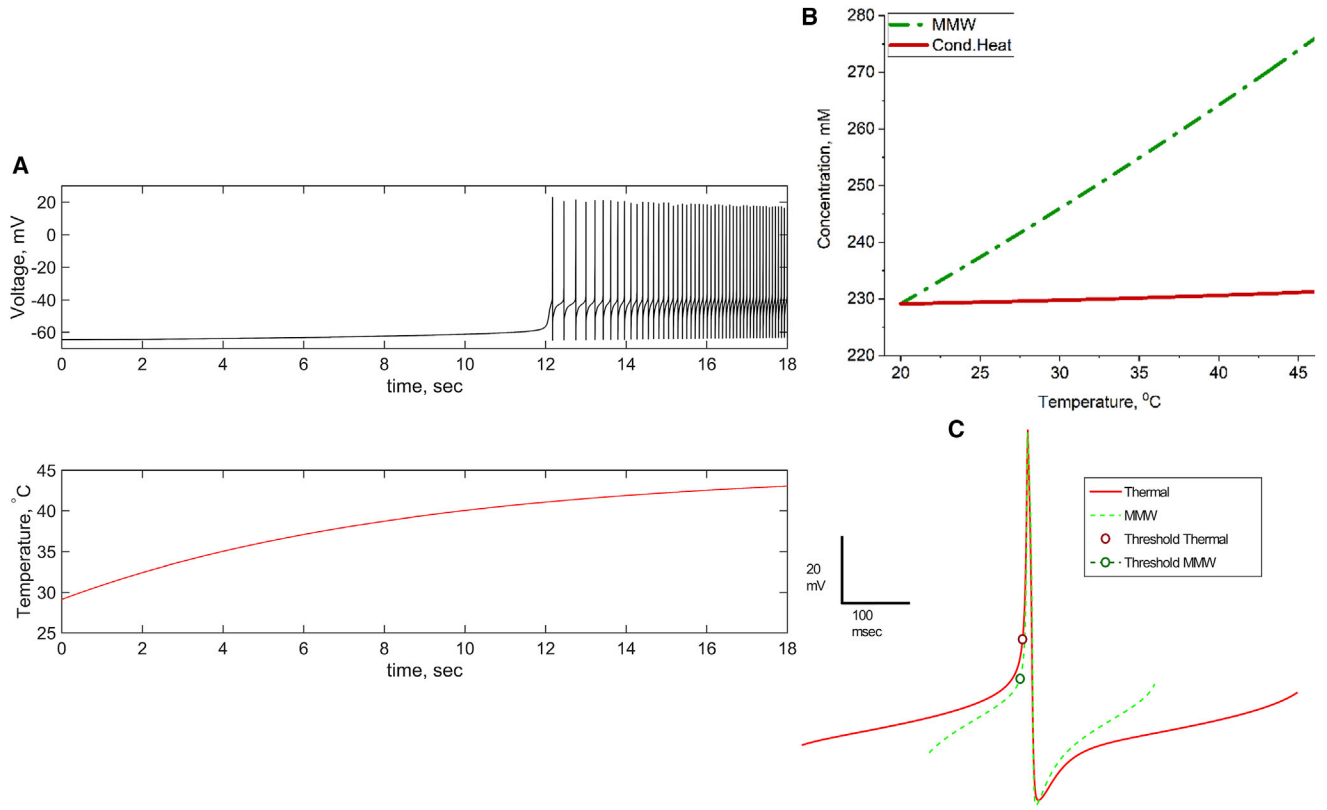

FIGURE 8 Computer simulation of Nl neuron model (NEURON) and the modeling of an ionic double layer on the surface of the membrane (Gouy-Chapman-Stern Model). (*A*) Shown are simulated traces of model Nl neuron response to a thermal stimulus; transmembrane voltage recorded from cell soma (*upper black trace*) and sample's temperature trace (*lower red trace*) are shown. (*B*) Calculated with Gouy-Chapman-Stern (G-Ch-S) model, changes in monovalent ion concentration on outer surface of membrane against temperature (*solid red line*) and with concurrent increase (up to 30%) of the surface charge density (*dot-dash green line*) are shown. The red solid line trace reflects the effect of thermal heating, whereas the green dot-dash line trace reflects the effect of MMW. (*C*) Shown are the simulated AP recorded from soma of Nl neuron model for simple temperature increase (*red solid line*, Therm.Heat.) and with concurrent increase of the surface charge density (*green dot-dash line*, MMW). Calculated AP activation thresholds are shown on each trace. Note that MMW trace has a lower activation threshold when compared with Therm.Heat., as observed in the real experiment. To see this figure in color, go online.

ions. The relationship between the system temperature and perimembrane sodium concentration is shown in Fig. 8 *B*. Within the temperature range we tested, the electrolyte concentration shifted only a few mM. Another factor defining potential and the local concentration of electrolyte on the membrane's surface is surface charge density (σ_{out}, σ_{in}). In contrast to the temperature, a 30% increase in σ_{out} caused nearly a 10 mV shift in surface potential and a 52 mM increase in surface electrolyte concentration (Fig. 8 *B*, MMW). Such strong changes could create conditions in close proximity to the membrane that are capable of sensitizing the TRPV1 via the osmosensing mechanism (52,55). Hence, the combined effect of increased temperature and surface charge density can have an additive impact that alters the TRPV1 activation threshold in Nl neurons. We have calculated the relationship between the local electrolyte concentration and the local temperature with concurrent relative alteration in surface charge density (Fig. 8 *B*, MMW). We find that only a 26% increase in surface charge density would satisfy the requirements for activating the Nl neuron. These conditions were inserted into our Nl neuron model by increasing the concentration of NaCl on the outer side of the membrane. The result shown in Fig. 8 *C* demonstrates an ~4 mV shift in the AP threshold of Nl neuron activation, which is similar to that observed in the experiments (Biological model). The simulation also demonstrated the increase in depolarizing inward TRPV1 current caused by the MMW type of heating (Fig. S10). Hence, among all potential mechanisms underlying the MMW irradiation effect, the most efficient one is simultaneous TRPV1 sensitization via its thermo- and osmosensitivity.

CONCLUSIONS

This study investigates the effect of MMW radiation on primary nociceptive neurons. By comparing the results of thermal heating and via more complex thermal and EM stimuli present in MMW irradiation, we have tried to elucidate and then assign specific electrophysiological changes to NI activation pathways. Understanding whether this form of

radiation (which generally does not occur in nature) and its potential effects on primary NIs is of vital importance.

In our experiments, we exploit the natural property of the NIs to detect and react to critical levels of thermal stimulus with a strong electrophysiological response. Indeed, thermosensitive NIs have specific vanilloid receptors (the most prominent being TRPV1) that can detect thermal stimuli above 38°C, which we have used in our experimental model. Thus, if the application of MMWs gives rise to a thermal response that deviates from the response caused by thermal heating, it would mean there are MMW-specific effects for at least some types of neurons.

Our core investigation compares the stimulation of Nl neurons with thermal heating and with exposure to MMWs with a power density of 170 mW/cm^2, in which we estimate approximately half the power is absorbed in the ganglion. We found that irradiating with MMWs facilitates the activation of Nl neurons, with the average voltage threshold for AP formation almost half that of thermal heating alone. We also measured a difference in the temperature of Nl activation (Fig. 4), but we cannot define the temperature within the neuron itself as the probe position only measures the surface temperature. Nevertheless, it would be reasonable to expect a decrease in the thermal threshold from a theoretical point of view. First, the lowered voltage threshold of AP activation would require a smaller activation current carried by the thermal sensor within the cell, TRPV1, thus shifting the thermal threshold to a lower temperature. Secondly, MMW-mediated sensitization to TRPV1 itself could lower the thermal activation threshold. These mechanisms are to be investigated in future studies.

We ran a series of tests to determine what could be behind this difference. For many types of sensory neurons (both vertebrate and annelids), the important regulatory mechanism for AP train formation is the calcium-dependent potassium current (K_{Ca}). Studies conducted on Vero kidney cells exposed to 42.25 GHz MMW radiation (16 mW) demonstrated a decrease in open-state probability for K_{Ca} channels (61). Hence, the slow process of depolarization accumulation after every AP would result in a decrease in the voltage threshold value. However, because of the temperature increase, any potential MMW effect on K_{Ca} channels open-state probability would be masked (a temperature increase facilitates the movement of the voltage sensor).

Heating itself commonly causes a significant increase in AP firing, activation, and inactivation of ion channels, changes in conduction velocity, synaptic events, etc. (62–64). In contrast to thermal heating, MMW irradiation does not have such an effect on AP formation when compared with control data. It implies that voltage-gated channels participating in AP formation may not be involved in changes in threshold but are governed by another mechanism; we postulated that this could be the TRPV1-like channel. To test our assumption, we performed an excitability study at room temperatures, in which TRPV1 is not involved. A comparison of the short current pulse protocol for MMW irradiation and control conditions revealed that MMW irradiation produces no significant alterations in the stimulatory current threshold, which is in agreement with our previous studies (14). Although conducted on different types of neurons, the study demonstrated that in contrast to mild thermal heating of the sample, low power exposure of Retzius neuron to MMW results in the suppression of AP firing. This result is consistent with what was seen in our experiments on Nl neurons subjected to MMW radiation (i.e., rather, slow "blip" firing of AP at the early stages of neuron activation). It is opposite to burst like firing in case of thermal heating, although the rate of sample heating should be considered.

We repeated the MMW irradiation and AP activation with a specific TRPV1 receptor antagonist (SB366791) in the bath solution; to our surprise, Nl neurons still responded to some extent to MMW irradiation. This implies that the activation of Nl neurons is not simply a result of activating the heat sensor of the TRPV1 receptor but a more complex phenomenon. Indeed, the SB366791 is an effective suppressor of the thermal and capsaicin-evoked responses in TRPV1-expressing cells, but it does not block the sensitivity to some other stimulus modalities (low pH, osmolarity) (49). Moreover, TRPV1 channels possess osmosensitivity properties, and this modality could be facilitated by, or be the facilitator of, thermal and chemical sensitivities (52). An alternative possibility is co-expression of TRPV1 and TRPV4 in the same neuron type in which those channels could successfully form heteromers that exhibit unique conductance and gating properties (65). In such a case, and especially from an electrophysiological point of view, we can still consider the entire complex structure as unitary.

In support of the assumption that thermal and osmosensitivity can be assigned to one sensory structure, we also tried MMW irradiation of Nm neurons, which did not show any analog to the neuronal activity alterations observed in the Nl neurons. This confirms the critical role of the TRPV1 receptors in the observed Nl sensitivity shifts. Hence, it is possible that MMWs sensitize the TRPV1 via the osmotic mechanism and thus activate the receptor. Indeed, the AP voltage threshold probability distributions for neurons subjected to MMW irradiation in the presence of the antagonist have a resemblance with probability distributions for thermal heating (Fig. 5, *C* and *D*). In either case, probability distributions consist of low (~0.5–8.5 mV) and high (~4.5–16 mV) voltage thresholds, but the probability of low voltage thresholds is much higher for antagonist-treated neurons. It is in accord with earlier MMW irradiation experiments (without SB366791), in which low voltage thresholds dominate. On the other hand, in experiments with an increased calcium concentration in the extracellular solution, when ion fluctuations in perimembrane space were buffered, only high voltage thresholds were observed. Hence, this suggests that MMW exposure could alter solute

concentration in the perimembrane space, and our observations are in accord with this condition.

To help us better understand the individual contributions from all the observed effects of MMW-irradiated Nl neurons, a mathematical model of our Nl neuron was constructed with NEURON simulation software. The model shows the collective effect of all postulated MMW-stimulated response mechanisms and separates them from the thermal heating effects on Nl neurons. The model demonstrates that, without the TRPV1 channel, the neuron could not generate AP trains, regardless of the background temperature. Incorporation of a TRPV1 channel with thermal sensitivity only resulted in the generation of an AP train as soon as the NI temperature crossed the thermal threshold (Fig. S11).

Our model shows that the osmotic sensitization of TRPV1 requires only a 17% increase in electrolyte concentration around the cell to cause a significant reduction (79%) in the Nl threshold. How can MMWs induce this change, and why is it not also caused by thermal heating? One possible explanation is that the MMW radiation might stimulate an increase in calcium ion activity, because of a very high specific absorption rate and as a result, dissociate the calcium from the membrane. Increased σ_{out} would quickly attract monovalent counter ions, which in the extracellular medium, is mainly sodium cations (Na^+). The growing concentration of Na^+ in a perimembrane space could be sensed by the TRPV1 osmosensor and promote sensitization. Monovalent cations do not compensate surface charge in the same manner as divalent ones because the binding constants of monovalent cations are one to two orders of magnitude less than those of divalent cations (46,47). Experiments with high calcium ion concentration support this conclusion because under these conditions, the sensitizing effect of MMW exposure was eliminated. It is estimated in our model that only a 26% increase in surface charge density would be enough to build up a 17% increase in cation concentration and, as a result, activate the TRPV1 receptor. Taking into account that under normal conditions, most of the membrane surface's negatively charged sites are occupied by calcium ions (48), a 26% increase in surface charge density is plausible. In support of this hypothesis, it has been shown that 42 GHz radiation at a power level of 35 mW/cm^2 caused translocation of negatively charged phosphatidylserine from the inner to the outer side of the cell membrane (5,66–69).

Finally, an increase in σ_{out} and an increase in the concentration of Na^+ in proximity to the membrane surface agree with our data for the step-current protocol for MMW irradiation, which are not different to control, in contrast to the observed thermal heating effect. Indeed, studies by Hille (59,70,71) demonstrate that increased monovalent ion concentrations promote a positive shift in cell surface potential and thus make membranes less excitable. Other researchers (72) also showed that an increased negative charge on the membrane surface promotes resting state stability.

In summary, this work has demonstrated significant changes in the functional properties of thermosensitive primary sensory neurons subjected to MMW radiation that differs from the impact of direct thermal heating. NIs subject to intense MMW stimuli showed a notable decrease in the voltage threshold of AP formation, compared to thermal heating. Experiments and simulations confirmed the central role of the TRPV1-like channel in the observed phenomena. We conclude that the distinctive impacts of MMW radiation on NI neurons are based on sensitization of a TRPV1-like channel and that the observed lower thermal NI activation threshold is a result of the combined action of temperature and perimembrane osmolarity. The latter could be considered as the distinctive nonthermal component of MMW irradiation effects on cells because this osmolarity sensitization is not present with thermal heating. This two-modality sensitization mechanism is likely transferrable to other types of neurons exposed to MMW radiation. This study may be of use when considering potential safety guidelines for MMWs. Furthermore, because MMW radiation can be directed and focused, its effects on AP thresholds may have potential uses in neurostimulation or chronic pain suppression (via the mechanism of tachyphylaxis).

SUPPORTING MATERIAL

Supporting Material can be found online at https://doi.org/10.1016/j.bpj.2019.04.021.

AUTHOR CONTRIBUTIONS

V.P.W. and S.R. conception and design of research. S.R. and S.F. performed experiments. S.R. and S.F. analyzed the data. S.R. performed NEURON and MATLAB simulations and performed finite difference time domain simulation. S.R., V.P.W., A.R.H., and L.H. interpreted the results of experiments. S.R., S.F., and V.P.W. prepared figures. S.R. and V.P.W. drafted the manuscript. A.R.H. and L.H. edited and revised manuscript. S.R., A.R.H., L.H., S.F., and V.P.W. approved the final version of manuscript.

ACKNOWLEDGMENTS

We are thankful to Dr. Victor Pikov (Medipace) for technical support and the sharing of some equipment with us during this research. We also thank Dr. Peter Siegel (California Institute of Technology) for discussions and reviewing of the manuscript.

This work was supported by a research grant (DP140101770) provided by the Australian Research Council. V.P.W. is the recipient of an Australian Research Council Future Fellowship (project number FT180100683) funded by the Australian Government.

REFERENCES

1. Kristensen, T. T., W. Withayachumnankul, …, D. Abbott. 2010. Modeling terahertz heating effects on water. *Opt. Express.* 18:4727–4739.
2. Mason, P. A., T. J. Walters, …, K. L. Ryan. 2001. Lack of effect of 94 GHz radio frequency radiation exposure in an animal model of skin carcinogenesis. *Carcinogenesis.* 22:1701–1708.

3. Nicolas Nicolaz, C., M. Zhadobov, …, Y. Le Drean. 2009. Absence of direct effect of low-power millimeter-wave radiation at 60.4 GHz on endoplasmic reticulum stress. *Cell Biol. Toxicol.* 25:471–478.
4. Romanenko, S., R. Begley, …, V. P. Wallace. 2017. The interaction between electromagnetic fields at megahertz, gigahertz and terahertz frequencies with cells, tissues and organisms: risks and potential. *J. R. Soc. Interface.* 14:20170585.
5. Zhadobov, M., N. Chahat, …, Y. Le Drean. 2011. Millimeter-wave interactions with the human body: state of knowledge and recent advances. *Int. J. Microw. Wirel. Technol.* 3:237–247.
6. Le Quément, C., C. N. Nicolaz, …, Y. Le Dréan. 2014. Impact of 60-GHz millimeter waves and corresponding heat effect on endoplasmic reticulum stress sensor gene expression. *Bioelectromagnetics.* 35:444–451.
7. Titova, L. V., A. K. Ayesheshim, …, O. Kovalchuk. 2013. Intense THz pulses cause H2AX phosphorylation and activate DNA damage response in human skin tissue. *Biomed. Opt. Express.* 4:559–568.
8. Titova, L. V., A. K. Ayesheshim, …, O. Kovalchuk. 2013. Intense THz pulses down-regulate genes associated with skin cancer and psoriasis: a new therapeutic avenue? *Sci. Rep.* 3:2363.
9. Habauzit, D., C. Le Quément, …, Y. Le Dréan. 2014. Transcriptome analysis reveals the contribution of thermal and the specific effects in cellular response to millimeter wave exposure. *PLoS One.* 9:e109435.
10. Walters, T. J., D. W. Blick, …, K. R. Foster. 2000. Heating and pain sensation produced in human skin by millimeter waves: comparison to a simple thermal model. *Health Phys.* 78:259–267.
11. Radzievsky, A. A., O. V. Gordiienko, …, M. C. Ziskin. 2008. Electromagnetic millimeter wave induced hypoalgesia: frequency dependence and involvement of endogenous opioids. *Bioelectromagnetics.* 29:284–295.
12. Usichenko, T. I., H. Edinger, …, F. Feyerherd. 2006. Low-intensity electromagnetic millimeter waves for pain therapy. *Evid. Based Complement. Alternat. Med.* 3:201–207.
13. Romanenko, S., P. H. Siegel, …, V. Wallace. 2016. Alterations in neuronal action potential shape and spiking rate caused by pulsed 60 GHz millimeter wave radiation. *In* Proceedings of the 41st International Conference on Infrared, Millimeter, and Terahertz waves. IRMMW-THz.
14. Romanenko, S., P. H. Siegel, …, V. Pikov. 2014. Effects of millimeter wave irradiation and equivalent thermal heating on the activity of individual neurons in the leech ganglion. *J. Neurophysiol.* 112:2423–2431.
15. Romanenko, S., P. H. Siegel, …, V. Pikov. 2013. Comparison of the effects of millimeter wave irradiation, general bath heating, and localized heating on neuronal activity in the leech ganglion. *Proc. SPIE.* 8585.
16. Pikov, V., X. Arakaki, …, P. H. Siegel. 2010. Modulation of neuronal activity and plasma membrane properties with low-power millimeter waves in organotypic cortical slices. *J. Neural Eng.* 7:045003.
17. Romanenko, S., P. H. Siegel, and V. Pikov. 2013. Microdosimetry and physiological effects of millimeter wave irradiation in isolated neural ganglion preparation. *In* Proceedings of the 2013 International Kharkov Symposium on Physics and Engineering of Microwaves, Millimeter and Submillimeter Waves, pp. 512–516.
18. Romanenko, S., P. H. Siegel, …, V. Wallace. 2017. Evaluation of a biologically relevant level of MMW radiation absorption in neuronal tissue. 2017. *In* 42nd International Conference on Infrared, Millimeter, and Terahertz Waves. IRMMW-THz Published online October 16, 2017. https://doi.org/10.1109/IRMMW-THz.2017.8066864.
19. Summers, T., S. Holec, and B. D. Burrell. 2014. Physiological and behavioral evidence of a capsaicin-sensitive TRPV-like channel in the medicinal leech. *J. Exp. Biol.* 217:4167–4173.
20. Wang, S., J. Joseph, …, M. K. Chung. 2015. Modality-specific mechanisms of protein kinase C-induced hypersensitivity of TRPV1: S800 is a polymodal sensitization site. *Pain.* 156:931–941.
21. Koerber, H. R., S. L. McIlwrath, …, B. M. Davis. 2010. Cutaneous C-polymodal fibers lacking TRPV1 are sensitized to heat following inflammation, but fail to drive heat hyperalgesia in the absence of TPV1 containing C-heat fibers. *Mol. Pain.* 6:58.
22. Nozadze, I., N. Tsiklauri, …, M. G. Tsagareli. 2016. Role of thermo TRPA1 and TRPV1 channels in heat, cold, and mechanical nociception of rats. *Behav. Pharmacol.* 27:29–36.
23. Planells-Cases, R., P. Valente, …, A. Szallasi. 2011. Complex regulation of TRPV1 and related thermo-TRPs: implications for therapeutic intervention. *Adv. Exp. Med. Biol.* 704:491–515.
24. Smith, E. S., and G. R. Lewin. 2009. Nociceptors: a phylogenetic view. *J. Comp. Physiol. A Neuroethol. Sens. Neural Behav. Physiol.* 195:1089–1106.
25. Safronov, B. V., V. Pinto, and V. A. Derkach. 2007. High-resolution single-cell imaging for functional studies in the whole brain and spinal cord and thick tissue blocks using light-emitting diode illumination. *J. Neurosci. Methods.* 164:292–298.
26. Nielsen, J., and L. Arendt-Nielsen. 1998. The influence of rate of temperature change and peak stimulus duration on pain intensity and quality. *Somatosens. Mot. Res.* 15:220–229.
27. Bertie, J. E., and Z. Lan. 2016. Infrared intensities of liquids XX: the intensity of the OH stretching band of liquid water revisited, and the best current values of the optical constants of H2O(l) at 25°C between 15,000 and 1 cm−1. *Appl. Spectrosc.* 50:1047–1057.
28. Explanations of the complex behavior of liquid water. *In* Water Structure and Science. M. Chaplin, ed. Creative Commons Attribution.
29. Schneider, C. A., W. S. Rasband, and K. W. Eliceiri. 2012. NIH Image to ImageJ: 25 years of image analysis. *Nat. Methods.* 9:671–675.
30. Ro/nne, C., L. Thrane, …, S. r. R. Keiding. 1997. Investigation of the temperature dependence of dielectric relaxation in liquid water by THz reflection spectroscopy and molecular dynamics simulation. *J. Chem. Phys.* 107:5319–5331.
31. Gabriel, S., R. W. Lau, and C. Gabriel. 1996. The dielectric properties of biological tissues: III. Parametric models for the dielectric spectrum of tissues. *Phys. Med. Biol.* 41:2271–2293.
32. Madjar, H. M. 2016. Human radio frequency exposure limits: An update of reference levels in Europe, USA, Canada, China, Japan and Korea. *In* Proceedings of the 2016 International Symposium on Electromagnetic Compatibility - EMC EUROPE, pp. 467–473.
33. Wu, T., T. S. Rappaport, and C. M. Collins. 2015. Safe for generations to come. *IEEE Microw. Mag.* 16:65–84.
34. Hines, M. L., and N. T. Carnevale. 2001. NEURON: a tool for neuroscientists. *Neuroscientist.* 7:123–135.
35. Hines, M. L., and N. T. Carnevale. 2000. Expanding NEURON's repertoire of mechanisms with NMODL. *Neural Comput.* 12:995–1007.
36. Hines, M. L., and N. T. Carnevale. 1997. The NEURON simulation environment. *Neural Comput.* 9:1179–1209.
37. Nicholls, J. G., and D. A. Baylor. 1968. Specific modalities and receptive fields of sensory neurons in CNS of the leech. *J. Neurophysiol.* 31:740–756.
38. Baccus, S. A. 1998. Synaptic facilitation by reflected action potentials: enhancement of transmission when nerve impulses reverse direction at axon branch points. *Proc. Natl. Acad. Sci. USA.* 95:8345–8350.
39. Genet, S., R. Costalat, and J. Burger. 2000. A few comments on electrostatic interactions in cell physiology. *Acta Biotheor.* 48:273–287.
40. Shapiro, M. G., K. Homma, …, F. Bezanilla. 2012. Infrared light excites cells by changing their electrical capacitance. *Nat. Commun.* 3:736.
41. Kuyucak, S., and S. H. Chung. 1994. Temperature dependence of conductivity in electrolyte solutions and ionic channels of biological membranes. *Biophys. Chem.* 52:15–24.
42. Stogryn, A. 1971. Equations for calculating the dielectric constant of saline water (correspondence). *IEEE Trans. Microw. Theory Tech.* 19:733–736.
43. Berg, R. W. 2015. Spike_threshold_PS(trace,dt,win, win2, Fc,factordvdt) In version 1.0.0.0. *mathworks.com* https://au.mathworks.com/matlabcentral/fileexchange/50999-spike_threshold_ps-trace-dt-win-win2-fc-factordvdt.

44. Sekerli, M., C. A. DelNegro, …, R. J. Butera. 2004. Estimating action potential thresholds from neuronal time-series: new metrics and evaluation of methodologies. *IEEE Trans. Bio. Med. Eng.* 51:1665–1672.

45. Romanenko, S., L. Hool, …, V. P. Wallace. 2018. The action potential (AP) activation threshold calculus. *GitHub* https://github.com/SergiiRv/ApctionPotentialThreshold.git.

46. Kostiuk, P. G., P. A. Doroshenko, and V. N. Ponomarev. 1980. [Surface charge in the region where the calcium channels of mollusk neuron somatic membrane are located]. *Dokl. Akad. Nauk SSSR.* 250:464–467.

47. Kostyuk, P. G., S. L. Mironov, …, V. N. Ponomarev. 1982. Surface charges on the outer side of mollusc neuron membrane. *J. Membr. Biol.* 70:171–179.

48. McLaughlin, S. 1989. The electrostatic properties of membranes. *Annu. Rev. Biophys. Biophys. Chem.* 18:113–136.

49. Gunthorpe, M. J., H. K. Rami, …, J. B. Davis. 2004. Identification and characterisation of SB-366791, a potent and selective vanilloid receptor (VR1/TRPV1) antagonist. *Neuropharmacology.* 46:133–149.

50. Cenac, N., C. Altier, …, N. Vergnolle. 2008. Transient receptor potential vanilloid-4 has a major role in visceral hypersensitivity symptoms. *Gastroenterology.* 135:937–946, 946.e1–e2..

51. Kamakura, T., M. Kondo, …, S. Shimada. 2016. Functional expression of an osmosensitive cation channel, transient receptor potential vanilloid 4, in rat vestibular ganglia. *Audiol. Neurotol.* 21:268–274.

52. Liedtke, W. 2006. Transient receptor potential vanilloid channels functioning in transduction of osmotic stimuli. *J. Endocrinol.* 191:515–523.

53. Coulon, P., H. J. Wüsten, …, P. W. Dierkes. 2008. Swelling-activated chloride channels in leech Retzius neurons. *J. Exp. Biol.* 211:630–641.

54. Kees, M. G., H. Schlotterbeck, …, P. Diemunsch. 2005. Le soluté de Ringer: un standard "isotonique" discutable. *Ann. Fr. Anesth. Reanim.* 24:653–655.

55. Nishihara, E., T. Y. Hiyama, and M. Noda. 2011. Osmosensitivity of transient receptor potential vanilloid 1 is synergistically enhanced by distinct activating stimuli such as temperature and protons. *PLoS One.* 6:e22246.

56. Plaksin, M., E. Kimmel, and S. Shoham. 2017. Correspondence: revisiting the theoretical cell membrane thermal capacitance response. *Nat. Commun.* 8:1431.

57. Hille, B. 1992. Axons, ions, and dons. *Science.* 258:144–145.

58. Hille, B. 1992. Pumping ions. *Science.* 255:742.

59. Hille, B., A. M. Woodhull, and B. I. Shapiro. 1975. Negative surface charge near sodium channels of nerve: divalent ions, monovalent ions, and pH. *Philos. Trans. R. Soc. Lond. B Biol. Sci.* 270:301–318.

60. Chandler, W. K., A. L. Hodgkin, and H. Meves. 1965. The effect of changing the internal solution on sodium inactivation and related phenomena in giant axons. *J. Physiol.* 180:821–836.

61. Geletyuk, V. I., V. N. Kazachenko, …, E. E. Fesenko. 1995. Dual effects of microwaves on single Ca(2+)-activated K+ channels in cultured kidney cells Vero. *FEBS Lett.* 359:85–88.

62. Warzecha, A., W. Horstmann, and M. Egelhaaf. 1999. Temperature-dependence of neuronal performance in the motion pathway of the blowfly calliphora erythrocephala. *J. Exp. Biol.* 202:3161–3170.

63. Zhao, Y., and J. A. Boulant. 2005. Temperature effects on neuronal membrane potentials and inward currents in rat hypothalamic tissue slices. *J. Physiol.* 564:245–257.

64. Thompson, S. M., L. M. Masukawa, and D. A. Prince. 1985. Temperature dependence of intrinsic membrane properties and synaptic potentials in hippocampal CA1 neurons in vitro. *J. Neurosci.* 5:817–824.

65. Kassmann, M., C. Harteneck, …, M. Gollasch. 2013. Transient receptor potential vanilloid 1 (TRPV1), TRPV4, and the kidney. *Acta Physiol. (Oxf.).* 207:546–564.

66. Yeung, T., G. E. Gilbert, …, S. Grinstein. 2008. Membrane phosphatidylserine regulates surface charge and protein localization. *Science.* 319:210–213.

67. van Dijck, P. W. M. 1979. Negatively charged phospholipids and their position in the cholesterol affinity sequence. *Biochim. Biophys. Acta.* 555:89–101.

68. Szabo, I., J. Kappelmayer, …, M. C. Ziskin. 2006. Millimeter wave induced reversible externalization of phosphatidylserine molecules in cells exposed in vitro. *Bioelectromagnetics.* 27:233–244.

69. Vincelette, R. L., C. C. Roth, …, B. L. Ibey. 2013. Thresholds for phosphatidylserine externalization in Chinese hamster ovarian cells following exposure to nanosecond pulsed electrical fields (nsPEF). *PLoS One.* 8:e63122.

70. Hille, B. 1968. Charges and potentials at the nerve surface. Divalent ions and pH. *J. Gen. Physiol.* 51:221–236.

71. Hille, B., E. J. Dickson, …, B. C. Suh. 2015. Phosphoinositides regulate ion channels. *Biochim. Biophys. Acta.* 1851:844–856.

72. Genet, S., R. Costalat, and J. Burger. 2001. The influence of plasma membrane electrostatic properties on the stability of cell ionic composition. *Biophys. J.* 81:2442–2457.